Eur Biophys J (2003) 31: 563–574
DOI 10.1007/s00249-002-0249-8

ARTICLE

David G. Regan · Philip W. Kuchel

Simulations of NMR-detected diffusion in suspensions of red cells: the "signatures" in *q*-space plots of various lattice arrangements

Received: 17 May 2002 / Revised: 27 July 2002 / Accepted: 2 August 2002 / Published online: 12 November 2002

Abstract Coherence effects from pulsed field-gradient spin-echo (PGSE) nuclear magnetic resonance diffusion experiments have been observed and characterized for diffusants in many heterogeneous systems, ranging from porous materials to cell suspensions. The resulting coherence patterns appear in plots of the normalized PGSE signal intensities as a function of the spatial wave vector **q** in a so-called *q*-space plot. The origin of these phenomena and their mathematical and physical underpinnings are now well established. We have conducted a number of studies of diffusion-coherence phenomena in suspensions of red blood cells and have made extensive use of computer simulations of molecular diffusion in virtual lattices of cells to aid in the interpretation and analysis of experimental data. In the current work we extended the canonical model used in these studies to investigate the effect that varying the packing arrangement of cells in the suspension has on the coherence patterns, as seen in *q*-space plots. We show that changes in the packing arrangement of cells are reflected in the *q*-space plots and in the results of diffusion tensor analysis and thus we speculate upon the possible clinical importance of these findings.

Keywords Diffusion tensor · Monte Carlo · Erythrocyte · Pulsed field-gradient spin-echo · *q*-Space plot

Abbreviations *DWI*: diffusion-weighted imaging · *Ht*: haematocrit · *MRI*: magnetic resonance imaging · *PGSE*: pulsed field-gradient spin-echo · *RBC*: red blood cell · *RBDG*: random binary digit generator · *RFPNG*: random floating point number generator · *RNG*: random number generator

D.G. Regan · P.W. Kuchel (✉)
School of Molecular and Microbial Biosciences,
University of Sydney, NSW 2006, Australia
E-mail: p.kuchel@mmb.usyd.edu.au
Fax: +61-2-93514726

Introduction

Pulsed field-gradient spin-echo (PGSE) nuclear magnetic resonance (NMR) is an expeditious and accurate method for measuring molecular diffusion in isotropic solution (Kärger et al. 1988). The method is based on the encoding of spatial information in the phase of spin magnetization, by the imposition of a magnetic field gradient on the sample, in order to measure positional displacement. Magnetic resonance imaging (MRI) also makes use of magnetic field gradients but in this case the spatial information is usually encoded in water spin density rather than the magnetization phase (Talagala and Lowe 1991). Increasingly, diffusion-weighted imaging (DWI) is being used clinically as a methodology but uses relative diffusion rates of water in the imaging of tissues.

In heterogeneous systems, PGSE NMR can yield diffraction and interference-like effects that arise as a result of spatial coherences in the magnetization phase in the sample (Mansfield and Grannell 1973). NMR diffusion-interference has been used to study the structure of porous media at a resolution inaccessible to conventional MRI (Callaghan et al. 1991) and we have shown that the PGSE method may also be used to study transport processes, cell morphology, and compartmentation in suspensions of red blood cells (RBCs) (Kuchel et al. 1997; Torres et al. 1998, 1999; Regan and Kuchel 2002).

These diffraction and interference-like effects, which are termed diffusion-coherence, can be visualized graphically by plotting the relative signal intensities from the PGSE NMR experiment as a function of the spatial wave vector **q** (units, m^{-1}):

$$\mathbf{q} = (2\pi)^{-1}\gamma\delta\mathbf{g} \tag{1}$$

where γ is the nuclear magnetogyric ratio, δ is the duration of each magnetic field-gradient pulse and **g** is the applied magnetic field-gradient vector. The *q*-space plot for a suspension of RBCs (which are aligned in the static

field, $\mathbf{B}_0$) (Kuchel et al. 1997, 2000) consists of a pore-hopping shoulder, which is due to water diffusing between the extracellular cavities (diffusion-interference), followed by a series of coherence peaks which are due to the restricted diffusion of water inside the cells (diffusion-diffraction) (Torres et al. 1999). The position of the pore-hopping shoulder in q-space plots is inversely related to the spacing of cells in the suspension, while the positions of the diffraction minima are inversely related to the average projected dimension of the cells in the direction in which the field-gradient has been imposed.

We have recently shown that the diffusion tensor of water in an RBC suspension, obtained from PGSE NMR diffusion measurements, provides information regarding the diffusion anisotropy of the sample and yields additional evidence of cell alignment in the magnetic field of the spectrometer (Kuchel et al. 2000). Diffusion tensor and q-space analysis are now being combined with conventional MRI (Basser et al. 1994; Basser 2002) to map fibre tracts in tissues such as the central nervous system (Basser and Pierpaoli 1996; Assaf and Cohen 1999; Pajevic and Pierpaoli 1999; Xue et al. 1999; Assaf and Cohen 2000).

In the present work we used computer simulations of diffusion, and combined diffusion tensor and q-space analysis of the theoretical data in a spectroscopic rather than imaging context. We set out to provide insights into q-space plots that would enable solution of the ''inverse problem'', whereby, from a q-space plot and minimal other information, the packing arrangement of uniform cells could be reconstructed.

The great advantage of both NMR imaging and spectroscopic methods for studying tissue structure and other properties is that they are non-invasive. Here we present an alternative and potentially useful technique for detecting changes in tissue structure using NMR and one that is capable of higher spatial resolution than conventional NMR imaging techniques.

Theory of methods

General

The work involved the computer simulation of molecular diffusion in three-dimensional lattices of cells. The method used a Monte Carlo random walk technique in the context of a PGSE NMR experiment. The output from the simulations was a set of calculated signal intensity values corresponding to the respective field-gradient strengths used in the simulation. The cells were assigned a biconcave disc shape (Fig. 1F) that closely approximates that of a human RBC. A ''unit cell'' consisted of a regular hexagonal prism containing a single RBC (Fig. 1F), both centered on the Cartesian origin. The unit cell was extended to a three-dimensional hexagonal lattice of unit cells (Fig. 1A) by the application of periodic boundary conditions. Layers of unit cells were offset with respect to one another in the x- and z-directions (Fig. 1A–C).

Random walks and random number generators

The Monte Carlo methods are so-named because of their utilization of sequences of uncorrelated random numbers. A Monte Carlo random walk simulates random molecular motion (viz., diffusion), and this representation is useful in exploring a binary tree, where it is necessary to emulate the random branching of a trajectory. Each step of a random walk involves executing a displacement (e.g., for diffusion, the displacement is of a particle in space and may be executed in one, two, or three dimensions) along a path whose direction is determined randomly by the generation of a random number.

Diffusion is brought about by the random motion of particles (molecules) due to thermally driven collisions. In an isotropic solution the mean-square distance traveled by molecules in an ensemble, in the time t, is given by the Einstein diffusion equation (Tanford 1961):

$$\langle r^2 \rangle = 6Dt \tag{2}$$

where r is the distance traveled by a single molecule and D is the diffusion coefficient. However, the exact analytical description of diffusion is difficult or impossible in a complex system such as a cell suspension which is compartmentalized (intra- and extracellular compartments) and in which the diffusant is exchanging between compartments, as has recently been reaffirmed by Jiang et al. (2001). The value of the apparent diffusion coefficient in a system such as this may vary as a function of its compartmental location. The difficulty of deriving an analytical solution, and the intrinsically stochastic nature of diffusion, make the Monte Carlo random walk an ideal method for exploring problems of this type.

The main element of the random walk simulation is a random number generator (RNG); the design of this algorithm is crucial to ensuring the absence of systematic bias in the final solution (Park and Miller 1988; Press and Teukolsky 1992; Knuth 1998). Any computer-generated sequence of numbers will be *pseudo-random* because no matter how large the period (i.e., the number of values generated in the sequence before the sequence repeats itself) the sequence will be predictable. An operational definition of randomness in the context of computer-generated sequences of numbers was suggested by Press et al. (1996): ''the deterministic program that produces a random sequence should be different from and – in all measurable respects – uncorrelated with the computer program that uses its output''. This implies that if any two different RNGs produce statistically different results when used in a particular program, then at least one of them is not a good generator.

Two RNGs were used in the present work: a random binary digit (or bit) generator (RBDG), whose output

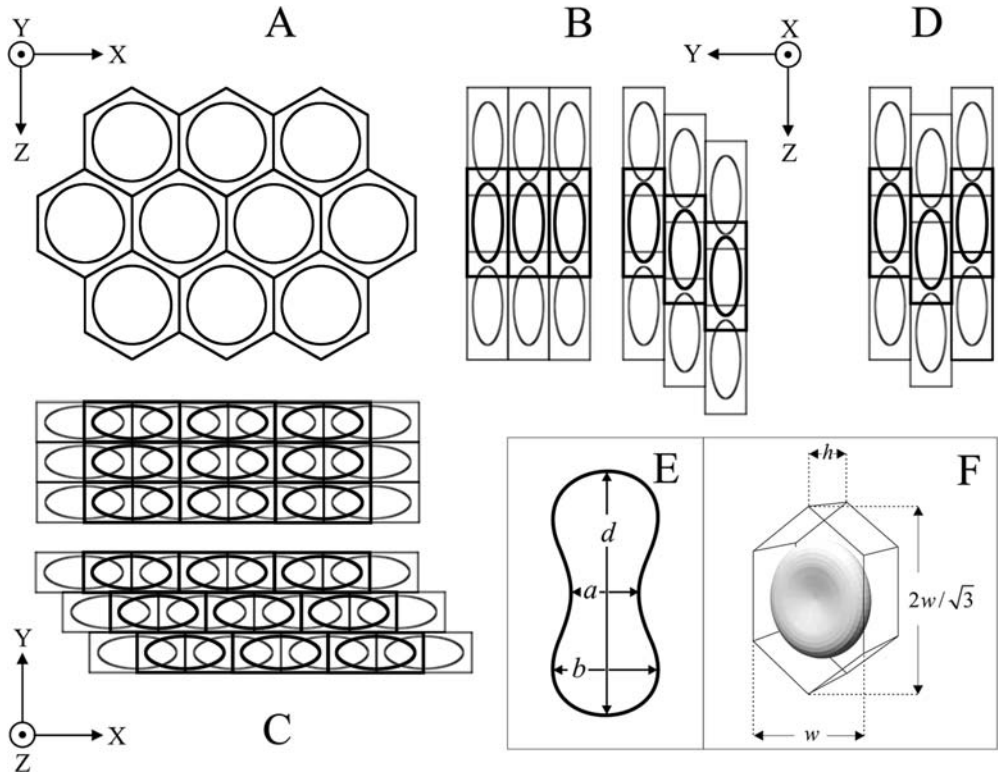

Fig. 1A–F Arrangement of virtual cells in the 3-D hexagonal lattice, the manner in which layers of unit cells are offset with respect to one another, and the geometry of the biconcave disc-shaped cell and the unit cell. The point of view of observation in **A**, **B**, **C**, and **D** in a Cartesian axis system is indicated by the *dot in a circle* (denoting a direction perpendicularly out of the page) and *arrow symbols*. **A** shows the arrangement of cells in a single layer of the hexagonal lattice. **B** and **C** show the manner in which adjacent layers of cells are offset with respect to one another in the *z*- and *x*-directions, respectively. **D** shows an alternative scheme for offsetting the layers; this scheme is not used in the work described in this paper. **E** is a schematic illustration of a cross-section of a biconcave disc through the axis of symmetry perpendicular to the disc planes; *a* is the minimum thickness of the disc in the dimpled region, *b* is the maximum thickness, and *d* is the main diameter. **F** shows the composition of the unit cell consisting of a hexagonal prism containing a biconcave disc-shaped RBC; *w* is the width of the prism and *h* is its depth

was either +1 or –1, and a random floating-point number generator (RFPNG), whose output was a double-precision floating point number between 0.0 and 1.0. Random binary digits were generated using a shift register generator (Knuth 1998), so named because the main step involves extracting the low-order bit of a *k*-bit word, where $k = 32$. This RBDG has been extensively tested by Tausworthe (1965), so is often referred to as a Tausworthe generator. The principal reasons for choosing this generator were computational speed and demonstrated statistical randomness. The RFPNG was used in the simulations for assigning random starting coordinates for random walk "trajectories" and for testing the condition for transition across the cell membrane. The algorithm was taken from Numerical Recipes in C (Press et al. 1996) and combines two different sequences obtained using a multiplicative congruential algorithm for maximum period (L'ecuyer 1988) with a Bays-Durham shuffle algorithm (Knuth 1998) for removing low-order serial correlations. To the best of our knowledge, these are the most robust and appropriate methods for the computer generation of random numbers for simulations of the type described here. While there is no perfect method[1], there were no systematic anomalies in the present model that were attributable to the RNGs.

Virtual cell

The model of the cell used in the simulations was a degree-four (quartic) surface (or cyclide; Fig. 1E and F), which closely approximates the shape of a human RBC (Kuchel and Fackerell 1999). This biconcave disc-shaped cell was chosen because NMR diffusion-coherence phenomena are reproducibly obtained from suspensions of these cells (Kuchel et al. 1997; Torres et al. 1998, 1999).

In Cartesian coordinates the surface is (Moon and Spencer 1988):

$$(x^2 + y^2 + z^2) - 2E(x^2 + z^2) - 2Fy^2 + G = 0 \qquad (3)$$

where the parameters *E*, *F*, and *G* are constants whose values are related to the shape in terms of its diameter *d*,

[1]The authors of this RNG contend that it provides perfect random numbers "within the limits of its floating point precision" and have offered $1000 to the designer of a statistical test that the generator fails in a "non-trivial way"

maximum thickness b, and minimum thickness a (Fig. 1E), such that (Kuchel and Fackerell 1999):

$$E = \frac{d^2}{4} - \frac{a^2}{4}\left(\frac{d^2}{b^2} - 1\right)\left[1 - \sqrt{1 - \frac{b^2}{a^2}}\right] \tag{4}$$

$$F = \frac{d^2}{b^2}E - \frac{b^2}{8}\left(\frac{d^4}{b^4} - 1\right) \tag{5}$$

$$G = d^2E - d^4/8 \tag{6}$$

The volume (V_{cell}) was calculated numerically using *Mathematica* (Wolfram Research, Champaign, Ill., USA). It involved evaluating the volume terms of the sum of the areas of slices taken parallel to the disc planes of the cell from its center to the beginning of the dimpled region and from the beginning of the dimpled region to the extremity of the disc. Thus:

$$V_1 = 2\pi \int_0^{b/2} \left(\sqrt{\left[(2y^2 - 2E)^2 - 4(y^4 - 2Fy^2 + G)\right]} - (2y^2 - 2E)\right)/2\,\mathrm{d}y \tag{7}$$

$$V_2 = 2\pi \int_{b/2}^{a/2} \sqrt{\left[(2y^2 - 2E)^2 - 4(y^4 - 2Fy^2 + G)\right]}\,\mathrm{d}y \tag{8}$$

$$V_{\text{cell}} = V_1 + V_2 \tag{9}$$

Spatial location

Following every step in the random walk it was necessary to determine whether the new coordinates denoted a position inside or outside the RBC. For a point molecule that has moved from P (x_1, y_1, z_1) to Q (x_2, y_2, z_2) in relation to a biconcave disc centered on O (0, 0, 0), a point A (x, y, z) is defined as the point of intersection between the displacement vector $\overrightarrow{\mathbf{OQ}}$ and the surface of the cell:

$$\overrightarrow{\mathbf{OA}} = \frac{t(x_2\mathbf{i} + y_2\mathbf{j} + z_2\mathbf{k})}{m} \tag{10}$$

where m and t denote the magnitude of $\overrightarrow{\mathrm{OQ}}$ and the relative position of A along $\overrightarrow{\mathrm{OQ}}$, respectively. Substituting the Cartesian coordinates of the point A (i.e., tx_2/m, ty_2/m, and tz_2/m) into Eq. (3) yields a quadratic in t^2:

$$\frac{t^4\left[x^4 + y^4 + z^4 + 2x^2y^2 + 2x^2z^2 + 2y^2z^2\right]}{m^4} - \frac{t^2\left[2E\left(x^2 + y^2\right) + 2Fy^2\right]}{m^2} + G = 0 \tag{11}$$

If $|t|t \geq m$, then the point Q lies inside the RBC, otherwise Q lies outside the RBC. In this latter case it was necessary to calculate the point of intersection between $\overrightarrow{\mathrm{PQ}}$ and the surface of the RBC. An analytical solution exists to this problem but involves the solution of a quartic expression yielding four solutions, which are tested to determine the physically correct one. For reasons of computational speed we used a numerical method to solve for the roots in this problem. The algorithm used a combination of the Newton-Raphson and bisection methods (Faires and Burden 1998). This method is particularly well suited to this problem since the solution is known to be bracketed in the small interval defined by $\overrightarrow{PQ}$. Mathematica was used to generate the necessary expressions[2], which owing to their length and complexity are not given here[3]. The computation converged rapidly (within a few iterations) to a solution of the specified accuracy.

Permeability and membrane transition

In the context of the Monte Carlo simulations of diffusion in cell suspensions, membrane permeability (P_{d}) is related to the probability of transition across the membrane, tp, by (Regan and Kuchel 2000):

$$tp = P_{\text{d}}s/D \tag{12}$$

where P_{d} (units, m s^{-1}) is the permeability of the membrane, s is the length of a single step in the random walk, and D is the intra- or extracellular diffusion coefficient. In order to test the condition for membrane transition, a random number was generated with the RFPNG and compared with the calculated value of tp; transition across the membrane was allowed if the generated number was less than tp.

Unit cell

The primary unit cell consisted of a regular hexagonal prism containing a virtual RBC (see Fig. 1E). For convenience, both objects were centered at the origin of a Cartesian coordinate system. The primary unit cell, and the application of periodic boundary conditions (described below), provided the basis for simulating diffusion in a three-dimensional lattice of RBC (a two-dimensional representation is given in Fig. 1A). The hexagonal prism was invoked in the simulations by specifying its boundaries in the xz- and yz-planes: $|x| \leq w/2$, $|y| \leq h/2$, and $|z| \leq (w - |x|)/\sqrt{3}$, where w is the distance separating the parallel sides of the prism in

[2]Two expressions were necessary for the Newton-Raphson algorithm: (1) an expression that equated the equation for the biconcave disc with the line segment defined by **PQ**; and (2) the first derivative of the former expression

[3]The code listings for these and all other algorithms described here are available on request from the authors

the x-direction, and h is the distance separating the hexagonal faces of the prism in the y-direction (see Fig. 1F).

The dimensions of the hexagonal prism were subjected to two constraints: (1) the volume, which is given by:

$$V_{\text{prism}} = 4w^2 h \sin(\pi/3) \tag{13}$$

conforms to:

$$V_{\text{prism}} = V_{\text{RBC}}/Ht, \tag{14}$$

ensuring that the desired haematocrit of the suspension is maintained for any value of cell volume; and (2) the distance separating the extremities of the disc planes and the edges of the disc from the surface of the prism are equal, viz.:

$$h - a = w - d \tag{15}$$

The analytical simultaneous solution of Eqs. (13, 14, 15) in *Mathematica* yielded formulae for calculating the values of w and h.

Diffusion tensor

In aqueous suspensions, human RBCs become aligned in a strong magnetic field with their disc planes parallel to the direction of the field (Higashi et al. 1993, 1996). The first evidence of alignment in the $\mathbf{B}_0$ field of an NMR spectrometer was obtained by using both q-space analysis (Kuchel et al. 1997) and subsequently by diffusion tensor analysis (Kuchel et al. 2000). The latter is based on the diffusion anisotropy that occurs as a result of the alignment of the disc-like cells.

The diffusion tensor, **D**, is second-rank with nine elements:

$$\mathbf{D} = \begin{pmatrix} D_{11} & D_{12} & D_{13} \\ D_{21} & D_{22} & D_{23} \\ D_{31} & D_{32} & D_{33} \end{pmatrix} \tag{16}$$

In order to determine the values of the elements in **D**, diffusion must be measured in at least six different directions, which in the case of the PGSE NMR method requires that the magnetic field gradients be applied in at least six different directions; this is readily achieved by using a modern triple-axis gradient probe which allows any combination of x-, y-, and z-gradients to be applied. Multivariate regression analysis is used to evaluate **D** (Kuchel et al. 2000) and the elements (D_{11}, D_{22}, D_{33}) of the diagonalized tensor are the estimates of the apparent diffusion coefficients in the x-, y-, and z-directions.

These estimates are generally dominated by the value for the intracellular water whose diffusion is severely restricted by the cell membrane. This results in a spin-echo signal that is attenuated less rapidly than the signal from the extracellular water. On the other hand, the extracellular water does contribute to the signal so the diffusion tensor should reflect differences in the way in which cells are arranged with respect to one another. In the simulations described here, layers of cells were offset in the x- and z-directions; hence it was anticipated that this would give rise to measurable differences in the diagonal elements of the respective diffusion tensors.

Methods

General

Molecular diffusion in lattices of RBCs was simulated as described above. Random walk trajectories for ensembles of point molecules in a three-dimensional lattice were used. Periodic boundary conditions were applied to a unit cell to simulate an infinite array, as described above (see Theory of methods: Unit cell). In addition to calculating the positional displacement of a point molecule at each step of the random walk, the phase[4] (ϕ) of the magnetic dipole moment vector (MDMV) was also calculated in the context of a PGSE NMR experiment. Various geometrical arrangements of the RBC were considered; layers of cells in the lattice were offset by different amounts with respect to each other in the x- and y- directions (Fig. 1A–C). The resulting list of relative signal intensities from each simulation was plotted as a function of the magnitude of **q**, in a q-space plot.

Monte Carlo simulations

The RFPNG was used to assign each random walk trajectory in an ensemble with a random starting position in the unit cell[5]. The ratio of trajectories with starting positions inside the biconcave disc to those with starting positions outside it (but inside the hexagonal prism) was therefore determined by the chosen value of Ht. The size (s) of each step (in a particular compartment, i.e., intra- or extracellular) in the random walk was identical and was calculated as a fraction (f) of either the smallest dimension of the cell (i.e., a) or the minimum distance separating cells (i.e., w–d), whichever was smaller. Previous work had shown that, for simulations of diffusion between perfectly reflecting parallel planes, the distance separating the planes must be at least $5s$ (Piton et al. 1993) for results to match the analytical solution (Tanner and Stejskal 1968). Using this as a guideline, f was assigned a value of 0.1. The duration of a single step was calculated using Eq. (2). For each step in the random walk the RBDG was used to assign a random direction in each of the x-, y-, and z-directions. The point molecule was thus displaced in these directions by a distance corresponding to the product of the output from the RBDG (± 1) and s.

Upon execution of each step of the random walk, it is necessary to determine whether the molecule is located inside or outside the biconcave disc and, in the case where it is outside the disc prior to the last jump, whether it has exited the hexagonal prism[6]. If the point molecule has moved from inside to outside the biconcave disc, or vice versa, the membrane transition condition is tested, and the point molecule either reflected back off the surface or allowed to cross the surface, depending on the outcome of the test. If the

[4]This phase relates to the angle between the projection of the magnetic dipole moment vector onto the xy-plane and the y-axis in the rotating frame of reference

[5]While in the work described here trajectories were assigned starting positions anywhere in the unit cell, the program also allows the user to specify whether to start all trajectories either inside or outside the biconcave disc. Point molecules can therefore be confined to either compartment by turning off membrane exchange

[6]The constraints on step size precluded a point molecule moving from inside the biconcave disc to a position outside the hexagonal prism, or vice versa, in a single step

point molecule has exited the hexagonal prism, the periodic boundary conditions are applied to place it back inside the prism, in the position it would have occupied in the adjacent prism, while keeping track of its real displacement (p). If the point molecule has exited the hexagonal prism in the y-direction (i.e., has moved into a unit cell in the adjacent layer; $|y| > h/2$), the user-specified offsets are applied in the x- and z-directions by moving the point molecule, with respect to the prism, by the amount of the offset. The offset in x is specified as a fraction of the width (w) of the prism and the offset in z as a fraction of its height ($2w/\sqrt{3}$). Figure 2 is a schematic illustration (for two adjacent layers) of the different offset arrangements used in the simulations, while Fig. 3 shows the result of one such arrangement for a real simulation.

The change in MDMV phase accumulated as a result of the overall displacement of the point molecule during its trajectory is calculated (for all values of magnetic field-gradient strength, g) by incrementing the phase change that occurs as a result of each step executed during the first gradient pulse of the PGSE sequence and decrementing those executed during the second refocusing pulse:

$$\phi(g) = \gamma g t p \tag{17}$$

These values are summed and averaged for the entire ensemble and the signal intensity (E) is calculated for all values of g, as the projection of the bulk magnetization vector onto the y-axis. This is given by:

$$E(g) = \cos \phi(g) \tag{18}$$

Parameter values

Simulation parameters

All simulations were for ensembles of 10^8 non-interacting point-molecule trajectories. The values of the intracellular and extracellular diffusion coefficients were 8×10^{-10} m^2 s^{-1} and 1.6×10^{-9} m^2 s^{-1}, respectively[7] The dimensions of the biconcave disc, a, b, and d, were 1.0×10^{-6}, 2.12×10^{-6}, and 8.0×10^{-6} m, respectively, yielding a volume of 8.6×10^{-17} m^3, in accordance with the measured value for human RBCs (Dacie and Lewis 1975). Membrane permeability was 6.1×10^{-5} m s^{-1}, as determined experimentally for human RBCs (Benga et al. 1990), and Ht was 0.5. The tolerance for the Newton-Raphson routine (see Theory of methods: Virtual cell) was calculated as $10^{-4}\times a$, which yielded 10^{-10} for all simulations described here. Layers of cells were offset in the x- and z-directions by a factor of 0.0, 0.2, 0.25, or 0.5 times the width and height of the hexagonal prism, respectively (see Fig. 2).

PGSE parameters

The values of the PGSE parameters used in the simulations were in accordance with those used when conducting experiments on real RBC suspensions (Kuchel et al. 1997; Torres et al. 1998, 1999; Regan and Kuchel 2002) using a 400 MHz (proton frequency) spectrometer and the standard PGSE pulse train: delay-90°-τ-180°-τ-acquire (Kärger et al. 1988). The duration of the magnetic field-gradient pulses (δ) was 2 ms, and the time interval separating the pulses (Δ) was 20 ms, giving a total "diffusion time" of 22 ms. A set of 96 values, linearly spaced between 0 and 9.9 T m^{-1}, constituted

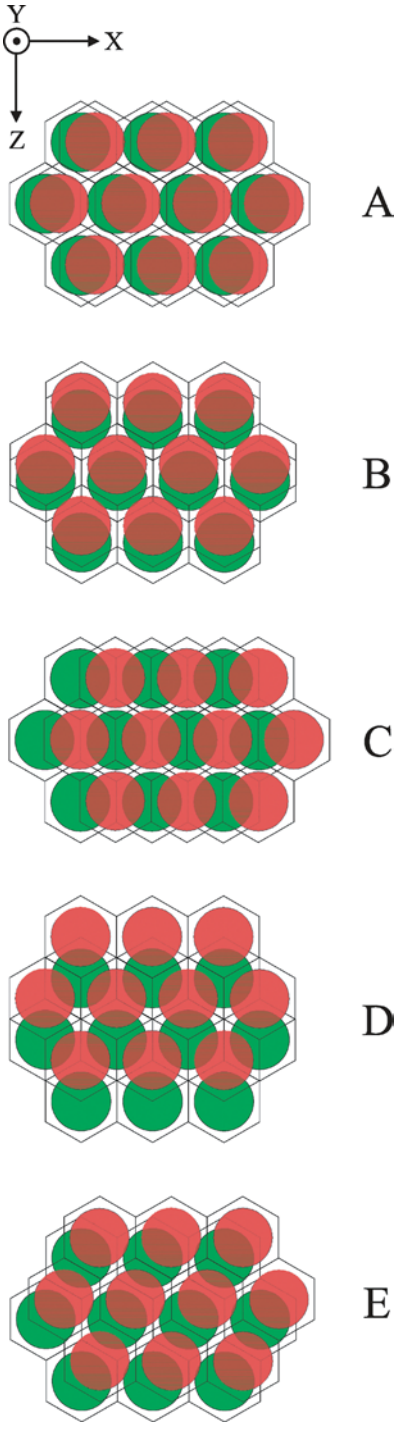

Fig. 2A–E Two-layer representations of the offset arrangements of layers of cells in the lattice used in the simulations. **A** offset of 0.2 in the x-direction; **B** offset of 0.2 in the z-direction; **C** offset of 0.5 in the x-direction; **D** offset of 0.5 in the z-direction; and **E** offset of 0.25 in both the x- and z-directions. No diagram is given for the arrangement in which the layers are not offset in either direction

[7]These values were based on the results of experimental results for water in RBC suspensions (unpublished data). While it was straightforward to measure the extracellular diffusion coefficient of water (using the standard PGSE NMR method), measuring the intracellular diffusion coefficient was more difficult owing to the restriction imposed by the cell membrane and the high concentration of haemoglobin with which water readily forms hydrogen bonds, hence greatly reducing its apparent value. However, we have shown that the value chosen for the simulations lies well within the range over which the mean residence time inside the cell is insensitive to the value of the diffusion coefficient, and is dependent on the exchange mediated by the aquaporins in the cell membrane (Regan and Kuchel 2000)

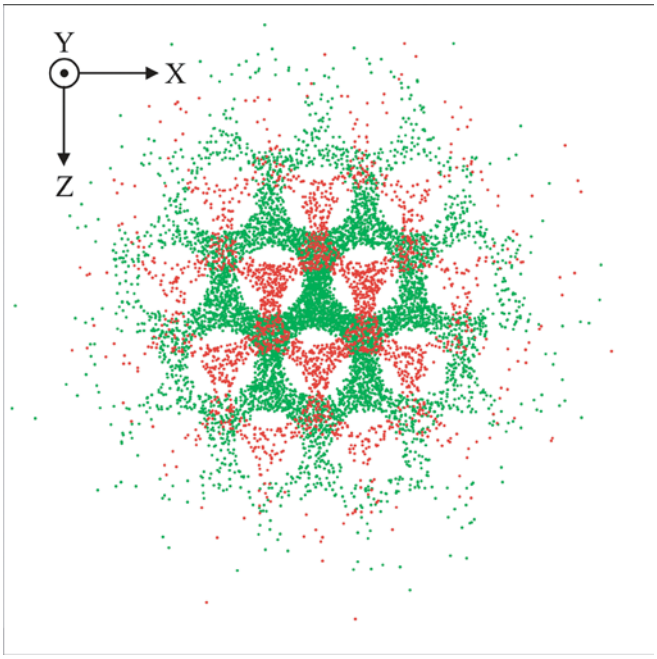

Fig. 3 Actual mapping of final coordinates from a simulation in which point molecules were confined to the extracellular space of the cell lattice (membrane permeability turned off and trajectories started outside the virtual cell) and layers were offset by 0.25 in both the *x*- and *z*-directions. The figure was generated using a program written in Matlab, which displayed final coordinates in thin slices through the centers of two adjacent layers parallel to the disc planes

the field-gradient strengths. The proton magnetogyric ratio was 2.675×10^8 rad s^{-1} T^{-1}.

Data analysis

Data from the simulations consisted of a set of signal intensities and a corresponding list of *q*-values. Matlab (Mathworks, Mass., USA) was used to apply a cubic spline to the data, which were then interpolated to increase the resolution from 96 to 1000 points[8]. *q*-Space plots were then generated from the interpolated data by using Origin (Microcal Software, Mass., USA) to plot the normalized signal intensities as a function of the magnitude of $\boldsymbol{q}$. A logarithmic ordinate scale was used to improve visualization of coherence features, which are otherwise difficult to discern as they occur at attenuation levels of 10^2 and greater (with the exception of the pore-hopping peak which occurs at lower levels of attenuation).

Matlab was used to calculate the elements of the diffusion tensor (from the raw data rather than from the interpolated data) using the method of Kuchel et al. (2000). Linear regression provided rough estimates of the terms of the tensor, which were then used as the initial estimates for calculating the final values, and confidence intervals by non-linear regression. The first five or six points only, lying in the region in which the data are of approximately single-exponential form, were included in the analysis.

[8]While very little overhead would be incurred by increasing the number of data points in the simulation from 96 to 1000 (i.e., the number of gradient values), this is not the case for the real PGSE NMR experiment in which a separate experiment is required for each data point. This method of improving data resolution, however, can be applied to both experimental and simulated data

Results

Simulations were conducted of diffusion of water in a three-dimensional hexagonal lattice of biconcave disc-shaped RBCs. Layers of cells were offset with respect to one another, as illustrated in Fig. 1A–C and Fig. 2. Figure 1D illustrates an alternative method for the offsetting of adjacent layers of cells but one that we did not employ. For all simulations, point molecules moved between the intra- and extracellular regions at the rate that we had determined experimentally for human RBC suspensions (see Methods: Parameter values). *q*-Space plots of diffusion in the *x*-, *y*-, and *z*-directions for all datasets (i.e., all alternative lattice arrangements) are shown in Fig. 4. A diffusion tensor was calculated for each dataset and the values of their diagonal elements are shown graphically in Fig. 5; these elements constitute estimates of the apparent diffusion coefficients in the *x*-, *y*-, and *z*-directions.

It is useful to introduce some specific notation to facilitate discussion of the results: the various lattice arrangements illustrated in Fig. 2 and described in Methods are referred to as follows: xO_xzO_z, where O_x and O_z are the fraction of the width or height of the unit cell, by which the layers of cells are offset in the *x*- and *z*-directions, respectively. For example $x0.25z0.25$ refers to an offset in the *x*-direction of 0.25 times the width of the hexagonal prism and an offset in the *z*-direction of 0.25 times its height.

Primarily for the purpose of discussing the results, simulations were also conducted for an $x0.0z0.2$ layer arrangement in which exchange was turned off (by setting the membrane permeability to 0.0 m s^{-1}); in other words, transition across the membrane could not occur. Three such simulations were conducted as follows: (1) diffusant in both the intra- and extracellular regions; (2) diffusant in the intracellular region only; and (3) diffusant in the extracellular region only. The *q*-space plots for these simulations, as well as for a previously published result (Regan and Kuchel 2002), in which there was no offsetting of layers (Fig. 6C, inset), are shown in Fig. 6.

Exchange on

x-Direction

The distinctive features of the *q*-space plots for diffusion measured in the *x*-direction (Fig. 4B) are as follows: (1) in the region of the pore-hopping shoulder (centered at $q=\sim0.9\times10^5$ m^{-1}) the curves were superimposed to a large extent, although it is possible to discern that the higher the offset values the flatter the shoulder, with the $x0.5z0.0$ and $x0.0z0.5$ curves being the flattest, and the $x0.0z0.0$ case having the most pronounced shoulder (see left inset of Fig. 4B); (2) the curves in the region of the first coherence peak (centered at $q=\sim2.3\times10^5$ m^{-1})

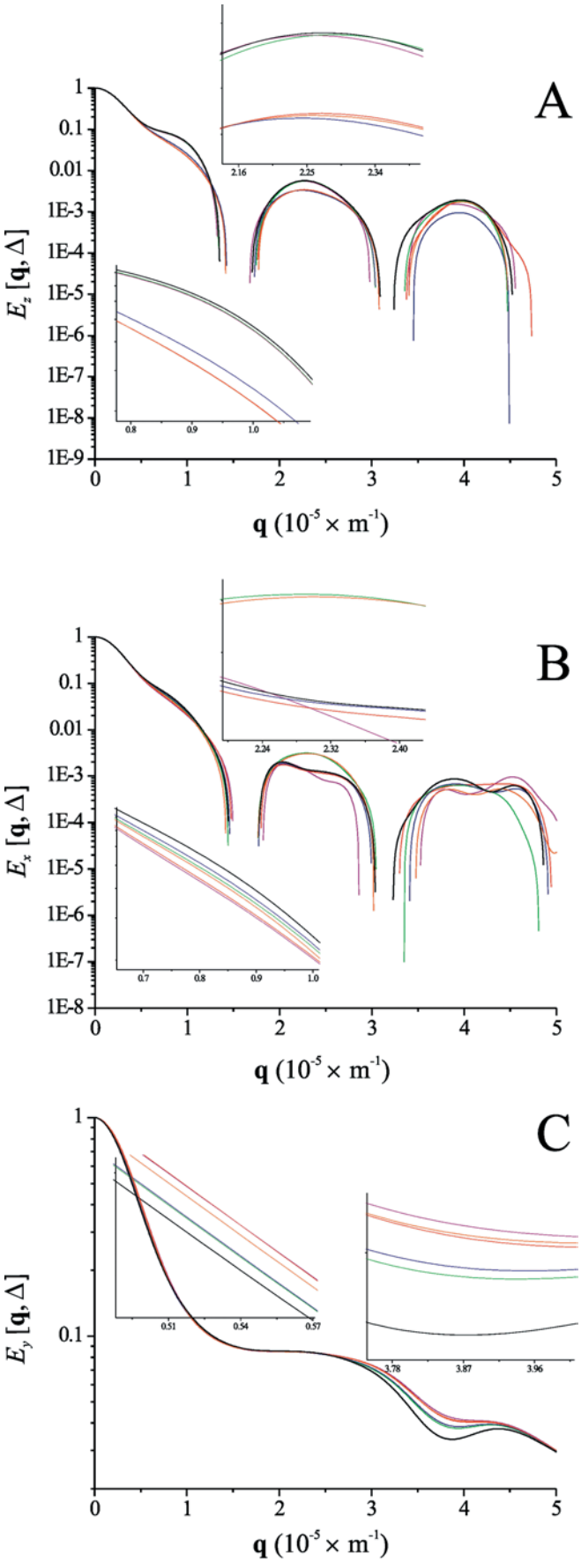

Fig. 4A–C *q*-Space plots from simulations of diffusion of water in suspensions of cells in which the layers of cells in a three-dimensional lattice were offset with respect to one another in the *x*- and *z*-directions. **A** diffusion measured in the *z*-direction; **B** diffusion measured in the *x*-direction; and **C** diffusion measured in the *y*-direction. In each of **A**, **B**, and **C** the *left inset* is a magnification of the region encompassing the center of the pore-hopping shoulder, and the *right inset* is a magnification of the region encompassing the center of the first coherence peak. *Key* (the notation used to represent the arrangement of layers is explained in Results): *black*, *x*0.0*z*0.0; *green*, *x*0.2*z*0.0; *blue*, *x*0.0*z*0.2; *orange*, *x*0.25*z*0.25; *crimson*, *x*0.5*z*0.0; *red*, *x*0.0*z*0.5

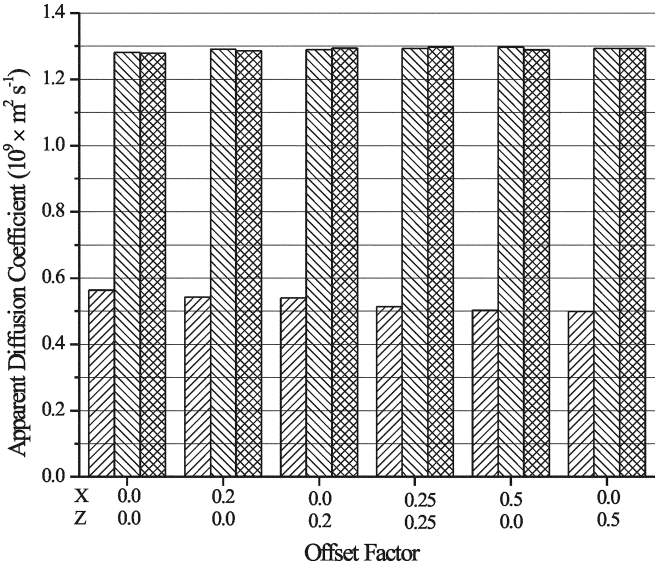

Fig. 5 Apparent diffusion coefficients measured in the *x*-, *y*-, and *z*-directions for simulations of diffusion of water in cell suspensions having different lattice arrangements. The values were obtained by calculating a diffusion tensor, as described in Theory of methods, and taking the diagonal terms. Each triplet of bars therefore represents the diagonal terms of the diffusion tensor for a particular offset arrangement, as indicated by the labeling beneath the abscissa. *Key*: *diagonally hatched*, *ascending from left to right*: diffusion measured in the *y*-direction; *diagonally hatched*, *descending from left to right*: diffusion measured in the *x*-direction; *cross-hatched*: diffusion measured in the *z*-direction

are almost superimposed for the pair *x*0.2*z*0.0 and *x*0.25*z*0.25 and for the triplet *x*0.0*z*0.0, *x*0.0*z*0.2, and *x*0.0*z*0.5, with *x*0.5*z*0.0 conforming more closely to the latter than the former (see right inset of Fig. 4B); (3) the previous grouping was also distinguished by a single peak for the pair (*x*0.2*z*0.0 and *x*0.25*z*0.25) and fine structure in the form of a double peak for the others (*x*0.0*z*0.0, *x*0.0*z*0.2, *x*0.0*z*0.5, and *x*0.5*z*0.0); and (4) the curves in the region of the second coherence peak (centered at $q = \sim 4.2 \times 10^5$ m^{-1}) all exhibit a degree of fine structure, although for *x*0.0*z*0.5 and *x*0.2*z*0.0 the peaks are more flattened than undulating.

Diffusion tensor analysis (see Fig. 5) revealed only small differences in the apparent diffusion coefficient in the *x*-direction for the different lattice arrangements. The lowest apparent diffusion coefficient was for

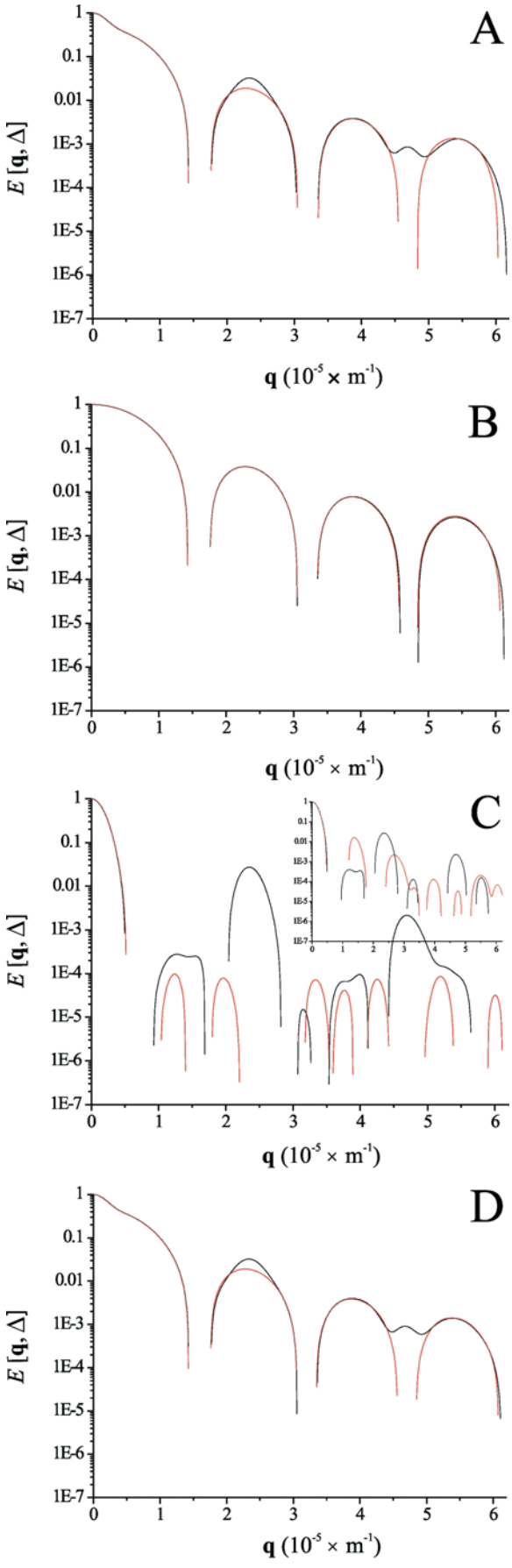

Fig. 6A–D *q*-Space plots for simulations of diffusion of water in an *x*0.0*z*0.2 lattice arrangement of cells in which exchange of water across the membrane was disabled by setting the permeability of the membrane to zero. *Key*: *black*, diffusion measured in the *x*-direction; *red*, diffusion measured in the *z*-direction. **A** water in both the intra- and extracellular regions; **B** water in the intracellular region only; **C** water in the extracellular region only; **C** *inset*: water in the extracellular region only and no offsetting of layers (i.e., *x*0.0*z*0.0); **D** the result of the superposition of **B** and **C**

*x*0.0*z*0.0 and the highest was for *x*0.5*z*0.0. In general, there was an increase in apparent diffusion coefficient as the amount of the offset was increased.

y-Direction

The *q*-space plots for diffusion in the *y*-direction (Fig. 4C) were distinct from those for diffusion in the *x*- and *z*-directions, which had similar graphical attributes. The curves for all datasets are almost indistinguishable except in the region of the minimum centered at $q = \sim 3.8 \times 10^5$ m^{-1}. In this region the curves are vertically separated into three clear groupings: *x*0.5*z*0.0, *x*0.0*z*0.5, and *x*0.25*z*0.25 are the least attenuated (*x*0.5*z*0.0, *x*0.0*z*0.5 are not distinguishable); *x*0.2*z*0.0 and *x*0.0*z*0.2 are attenuated to an intermediate extent; and *x*0.0*z*0.0 alone is attenuated to the greatest extent (see right inset of Fig. 4C). A similar separation can be discerned in the initial region of the curves centered at $q = \sim 0.5 \times 10^5$ m^{-1} (see left inset of Fig. 4C).

A clear trend is evident in the values of the apparent diffusion coefficients obtained from diffusion tensor analysis (Fig. 5). As the offset was increased the apparent diffusion coefficient in the *y*-direction became smaller. The extent of this decrease in the value of the apparent diffusion coefficient was higher for offsets in the *z*-direction than for equivalent offsets in the *x*-direction.

z-Direction

The *q*-space plots for diffusion in the *z*-direction (Fig. 4A) show a very clear grouping in both the region of the pore-hopping peak (at $q = \sim 0.9 \times 10^5$ m^{-1}; see left inset of Fig. 4A) and in the region of the first coherence peak (at $q = \sim 2.3 \times 10^5$ m^{-1}; see right inset of Fig. 4A). In these regions there is a significant vertical separation between the curves for the *x*0.0*z*0.0, *x*0.5*z*0.0, and *x*0.2*z*0.0 lattice arrangements and those for *x*0.0*z*0.2, *x*0.25*z*0.25, and *x*0.0*z*0.5. Within each grouping there is very little separation between the curves. In contrast to the curves for diffusion in the *x*-direction, there is no significant fine structure (double peaks) in the regions of the first or second coherence peak (centered at $q = \sim 4.0 \times 10^5$ m^{-1}).

As for diffusion in the *x*-direction, the apparent diffusion coefficients in the *z*-direction obtained from

diffusion tensor analysis show only small differences for the various lattice arrangements (Fig. 5). The smallest value of apparent diffusion coefficient occurred for $x0.0z0.0$, as was the case for diffusion in the x-direction; however, the highest value occurred for $x0.25z0.5$, whereas the highest value in the x-direction was for $x0.5z0.0$.

Exchange off

Figure 6 shows the q-space plots for three simulations, in an $x0.0z0.2$ lattice arrangement, in which exchange across the membrane was disabled by making the membrane impermeable. The figure illustrates that when the signal is obtained exclusively from the intracellular water (Fig. 6B), the q-space plots for the x- and z-directions are virtually indistinguishable. However, when the signal is obtained exclusively from the extracellular water (Fig. 6C), substantial differences in the q-space plots emerge in the form of fine structure in the coherence peaks for the x-direction, coupled with greatly varying levels of signal intensity. The inset of Fig. 6C shows the result of an earlier analogous simulation in which exchange was disabled but in which no offsetting of layers was implemented (i.e., an $x0.0z0.0$ lattice arrangement). Figure 6A shows the q-space plot for water diffusing in both the intra- and extracellular spaces simultaneously with exchange disabled, and although the signal is clearly dominated by the signal from the intracellular water, differences in the form of fine structure for diffusion in the x-direction are observed. Figure 6D was generated by combining the signals from the simulations in which water was confined to either the intra- or extracellular region. As expected, it is identical to the q-space plot for water diffusing in both regions simultaneously (Fig. 6A). It is important to note that the simulations used to generate Fig. 6A–C were entirely independent simulations, whereas Fig. 1D was generated by combining the results of the simulations that were used to generate Fig. 6B and C (i.e., it is not the result of an independent simulation). It is also noteworthy that Fig. 6A was generated from a simulation in which 10^8 point-molecule trajectories were recorded, while Fig. 6D was effectively generated from two such simulations so it was the result of 2×10^8 point-molecule trajectories.

Discussion

A number of general comments can be made regarding the results of the diffusion tensor and q-space analysis. First, the differences in apparent diffusion coefficients obtained from diffusion tensor analysis for the various lattice arrangements are very small. This is particularly true for the x- and z-directions, and although definite trends can be discerned, these are not likely to be discernible in real experimental data; the differences for the y-direction, however, are larger and the trend more apparent. Second, very clear differences are observed in the q-space plots for the various lattice arrangements and this in itself is significant as it suggests an alternative non-invasive method for detecting or monitoring changes in tissues that are of an intrinsically ordered nature. Third, while the q-space plots for all lattice arrangements are separately resolved, a loose grouping is apparent which may be explained on the basis of the topology of the extracellular region (see below). Fourth, the q-space plots for diffusion in the x-direction are discernibly different from those for diffusion in the z-direction and this can also be explained in terms of differences in the extracellular topology. A more detailed examination of these observations follows.

Exchange off

It is useful at this point to discuss the results obtained for diffusion in the absence of exchange, as illustrated in Fig. 6. These results show first and most importantly that differences in the q-space plots for diffusion in the x- and z-directions arise as a result of signals obtained from the extracellular water (Fig. 6C); no differences are observed for simulations in which water is diffusing in the intracellular region only (Fig. 6B). While the intracellular water experiences identical topology, regardless of its x- and z-components of diffusional direction, this is not the case for the extracellular water. As is illustrated in Fig. 7, water moving from one pore to another nearest-neighbor pore experiences two fundamentally different topologies: (1) the topology illustrated by the yellow and red shaded regions (which are symmetrically identical) implies an overall displacement having both x-and z-components of direction; and (2) the topology illustrated by the green shaded region which implies an

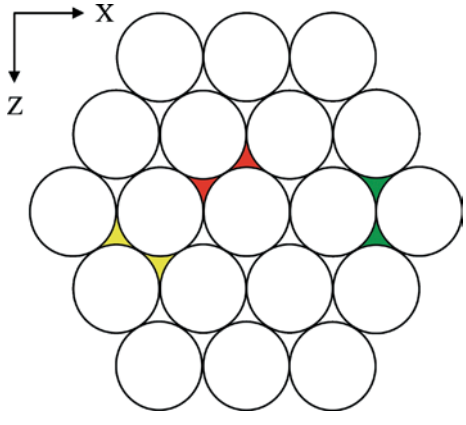

Fig. 7 Illustration of the different nearest-neighbor pore structures. The *red and yellow shaded regions* are symmetrically equivalent pore structures while the *green shaded region* is unique in its orientation. Transitions between nearest-neighbor pores in the x-direction are limited to transitions between pores of a single shape (those illustrated by the equivalent *red and yellow shaded regions*), while measured in the z-direction transitions can also occur between nearest-neighbor pores of the shape illustrated by the *green shaded region*

overall displacement in the z-direction only. It is therefore to be expected that the signal arising from the extracellular water will be different when measured in the x-direction than when measured in the z-direction.

The fact that Fig. 6D (obtained by superimposing the data from the separate simulations of intra- and extracellular water) is identical to Fig. 6A (simultaneous simulation of intra- and extracellular water in the absence of exchange) demonstrates that in the absence of exchange the overall signal is simply a superposition of the signals from the intra- and extracellular water; the composition of the overall signal is far more complex when exchange is introduced. This outcome is also predicted by the approximate analysis of Jiang et al. (2001).

Figure 6 also illustrates two other important points: (1) the overall signal is dominated by the signal from the intracellular water – this is because diffusion inside the cell is more restricted, resulting in a smaller apparent diffusion coefficient and the signal is consequently attenuated to a lesser degree than its extracellular counterpart for a given q-value; and (2) as illustrated by the inset of Fig. 6C (extracellular water, $x0.0z0.0$ lattice arrangement), different lattice arrangements give rise to q-space plots that are clearly different (although they contain similar gross features) and this can be attributed to the differences in the extracellular topology.

Exchange on

When exchange is introduced to the system, the PGSE signal is no longer the simple superposition of the intra- and extracellular signals but contains information relating to the rate at which the exchange is occurring. Additionally, while the topology of the extracellular region is fundamentally the same as described above for the non-exchanging system (and similarly is altered by changing the lattice arrangement), the boundaries of this topology are ''blurred'' by the exchange process. It is in accordance with expectation, therefore, that the q-space plots for the exchanging system are quite different from those of the non-exchanging one. The non-exchanging system, however, serves to identify the source of the fine structure observed in the exchanging one.

The complex nature of the exchanging system, combined with the complex topologies of the extracellular regions associated with each of the different lattice arrangements, makes it difficult to quantitatively interpret the different groupings and the fine structure described in Results. However, we can declare that the differences in the groupings are attributable to general differences in the three-dimensional topology of the extracellular region, while the fine structure observed in q-space plots for diffusion in the x-direction, but absent from those for diffusion in the z-direction, is due to the specific differences in the topology in those directions as described above (Discussion: Exchange off) and illustrated in Fig. 7.

The groupings observed for diffusion in the y-direction are more amenable to physical interpretation because, with reference to Fig. 2, we can more easily visualize the effect that offsetting the layers has on water diffusing in that direction. As the layers of cells are offset, part of the lattice that had a clear unimpeded path to diffusion for extracellular water in the y-direction becomes (partially) occluded by cells. Clearly, the $x0.0z0.0$ lattice arrangement (not shown in Fig. 2 but implied in Fig. 1A) provides the least impeded path to diffusion in the y-direction and therefore the highest attenuation of the PGSE signal. The lattice arrangements that offer the greatest impediment to diffusion in the y-direction are the $x0.5z0.0$, $x0.0z0.5$, and $x0.25z0.25$ arrangements and consequently the attenuation of the signal was the lowest in the q-space plots for these simulations. The $x0.2z0.0$ and $x0.0z0.2$ arrangements offer a similar and intermediate impediment to diffusion in the y-direction and this is reflected in an intermediate degree of signal attenuation.

The estimates of the apparent diffusion coefficients obtained from the diffusion tensors for the different lattice arrangements (see Fig. 5) are coarse because they constitute an average value that is weighted according to the relative contributions of the intra- and extracellular water signals. Although the Ht of the suspension was 0.5, the overall signal was dominated by the intracellular water whose intrinsic diffusion coefficient was smaller (to reflect the more viscous intracellular environment) and whose diffusion was more restricted (by the confinement of the cell membrane); the signal from the extracellular water was therefore attenuated to a greater extent at all given q-values as a result of its overall faster diffusion. It is therefore expected that it would be difficult to discern large differences in the apparent diffusion coefficients because changes in the lattice arrangement only affects the extracellular water. It is also not surprising that the most significant differences were observed for diffusion in the y-direction, because as the layers are moved relative to each other, the path an extracellular water molecule takes will be most changed in that direction. The trend that is observed for the y-direction, namely a reduced apparent diffusion coefficient as the offset is increased and a greater reduction for offsets in the z-direction, can be understood by referring to Fig. 2: the degree to which diffusion is restricted in the y-direction correlates very closely with the amount of white space, which constitutes the degree to which water is free to move in that direction. As the layers are moved with respect to one another the cells in each layer occlude, or eclipse, the path in the y-direction to some extent and this is reflected in the apparent diffusion coefficient.

Conclusions

We have shown that differences in the arrangement of layers in the simulated RBC lattice are reflected in the form of the respective q-space plots and in the values of

the apparent diffusion coefficients obtained from diffusion tensor analysis; hence the notion of "signatures" of cellular arrangements in the q-space plots. For diffusion in the x- and z-directions, these differences are primarily attributable to changes in the three-dimensional topology of the extracellular region. For diffusion in the y-direction, the differences are attributable mainly to the varying degree to which diffusion is impeded by offsetting the layers of cells. Future work will involve refining the analysis of the fine details and features present in the q-space plots and in obtaining more precise diffusion tensor data for the x- and z-directions. The computational methods and insights described here, however, constitute a means of understanding this novel and non-invasive NMR-based approach. It has potential applications in monitoring changes in the morphology of cells in suspensions and in solid tissues that normally display a degree of order in the arrangement of their layers of cells.

Acknowledgements The work was supported by a Project Grant to P.W.K. from the Australian Research Council. D.G.R. was supported by an Australian Postgraduate Award. Mr. Bill Lowe is thanked for general technical assistance. A/Prof. Russell Standish, Director of the High Performance Computing Support Unit at the University of New South Wales, is thanked for assistance in obtaining resource allocation on the APAC (Australasian Partnership for Advanced Computing) National Facility supercomputer, and in software implementation.

References

Assaf Y, Cohen Y (1999) Structural information in neuronal tissue as revealed by q-space diffusion NMR spectroscopy of metabolites in bovine optic nerve. NMR Biomed 12:335–344

Assaf Y, Cohen Y (2000) Assignment of the water slow-diffusing component in the central nervous system using q-space diffusion MRS: implications for fiber tract imaging. Magn Reson Med 43:191–199

Basser PJ (2002) Relationships between diffusion tensor and q-space MRI. Magn Reson Med 47:392–397

Basser PJ, Pierpaoli C (1996) Microstructural and physiological features of tissues elucidated by quantitative-diffusion-tensor MRI. J Magn Reson B 111:209–219

Basser PJ, Mattiello J, LeBihan D (1994) MR diffusion tensor spectroscopy and imaging. Biophys J 66:259–267

Benga G, Pop VI, Popescu O, Borza V (1990) On measuring the diffusional water permeability of human red blood cells and ghosts by nuclear magnetic resonance. J Biochem Biophys Methods 21:87–102

Callaghan PT, Coy A, MacGowan D, Packer KJ, Zelaya FO (1991) Diffraction-like effects in NMR diffusion studies of fluids in porous solids. Nature 351:467–469

Dacie JV, Lewis SM (1975) Practical haematology, 5th edn. Churchill Livingstone, London

Faires JD, Burden R (1998) Numerical methods, 2nd edn. Brooks/Cole, Pacific Grove, Calif

Higashi T, Yamagishi A, Takeuchi T, Kawaguchi N, Sagawa S, Onishi S, Date M (1993) Orientation of erythrocytes in a strong static magnetic field. Blood 82:1328–1334

Higashi T, Sagawa S, Ashida N, Takeuchi T (1996) Orientation of gluteraldehyde-fixed erythrocytes in strong static magnetic fields. Bioelectromagnetics 17:335–338

Jiang P-C, Yu T-Y, Perng W-C, Hwang L-P (2001) Pore-to-pore hopping model for the interpretation of the pulsed gradient spin echo attenuation of water diffusion in cell suspension systems. Biophys J 80:2493–2504

Kärger J, Pfeifer H, Heink W (1988) Principles and application of self-diffusion measurements by nuclear magnetic resonance. Adv Magn Reson 12:1–89

Knuth DE (1998) Seminumerical algorithms The art of computer programming, vol 2. Addison-Wesley-Longman, Reading, Mass., pp 1–193

Kuchel PW, Fackerell ED (1999) Parametric-equation representation of biconcave erythrocytes. Bull Math Biol 61:209–220

Kuchel PW, Coy A, Stilbs P (1997) NMR "diffusion-diffraction" of water revealing alignment of erythrocytes in a magnetic field and their dimensions and membrane transport characteristics. Magn Reson Med 37:637–643

Kuchel PW, Durrant CJ, Chapman BE, Jarrett PS, Regan DG (2000) Evidence of red cell alignment in the magnetic field of an NMR spectrometer based on the diffusion tensor of water. J Magn Reson 145:291–301

L'ecuyer P (1988) Efficient and portable combined random number generators. Commun ACM 31:742–751

Mansfield P, Grannell PK (1973) NMR 'diffraction' in solids? J Phys C Solid State Phys 6:L422–L426

Moon P, Spencer DE (1988) Field theory handbook, including coordinate systems, differential equations and their solutions. Springer, Berlin Heidelberg New York

Pajevic S, Pierpaoli C (1999) Color schemes to represent the orientation of anisotropic tissues from diffusion tensor data: application to white matter fiber tract mapping in the human brain. Magn Reson Med 42:526–540

Park SK, Miller KW (1988) Random number generators: good ones are hard to find. Commun ACM 31:1192–1201

Piton MC, Gilbert RG, Chapman BE, Kuchel PW (1993) Diffusion of oligomeric species in polymer solutions. Macromolecules 26:4472–4477

Press WH, Teukolsky SA (1992) Portable random number generators. Comput Phys 6:522–524

Press WH, Teukolsky SA, Vetterling WT, Flannery BP (1996) Numerical recipes in C, 2nd edn. Cambridge University Press, Cambridge

Regan DG, Kuchel PW (2000) Mean residence time of molecules diffusing in a cell bounded by a semi-permeable membrane: Monte Carlo simulations and an expression relating membrane transition probability to permeability. Eur Biophys J 29:221–227

Regan DG, Kuchel PW (2002) Simulations of molecular diffusion in lattices of cells: insights for NMR of red blood cells. Biophys J 83:161–171

Talagala SL, Lowe IJ (1991) Introduction to magnetic resonance imaging. Concepts Magn Reson 3:145–159

Tanford C (1961) Physical chemistry of macromolecules. Wiley, New York

Tanner JE, Stejskal EO (1968) Restricted self-diffusion of protons in colloidal systems by the pulsed-gradient, spin-echo method. J Chem Phys 49:1768–1777

Tausworthe RC (1965) Random numbers generated by linear recurrence modulo two. Math Comput 19:201–205

Torres AM, Michniewicz RJ, Chapman BE, Young GAR, Kuchel PW (1998) Characterisation of erythrocyte shapes and sizes by NMR diffusion-diffraction of water: correlations with electron micrographs. Magn Reson Imaging 16:423–434

Torres AM, Taurins AT, Regan DG, Chapman BE, Kuchel PW (1999) Assignment of coherence features in NMR q-space plots to particular diffusion modes in erythrocyte suspensions. J Magn Reson 138:135–143

Xue R, van Zijl PCM, Crain BJ, Solaiyappan M, Mori S (1999) In vivo three-dimensional reconstruction of rat brain axonal projections by diffusion tensor imaging. Magn Reson Med 42:1123–1127